International Journal of Bioprinting

RESEARCH ARTICLE

Multimaterial and multiscale scaffold for engineering enthesis organ

Simone Micalizzi[1†], Lara Russo[2†], Chiara Giacomelli[2], Francesca Montemurro[1], Carmelo de Maria[1], Martina Nencioni[2], Laura Marchetti[2], Maria Letizia Trincavelli[2], Giovanni Vozzi[1*]

[1]Research Centre E. Piaggio and Department of Information Engineering, University of Pisa, Largo L. Lazzarino 1, 56126 Pisa, Italy

[2]Department of Pharmacy, University of Pisa, Pisa 56127, Italy

(This article belongs to the *Special Issue: Bioprinting-based strategies for regenerative medicine, drug development and food technology applications*)

Abstract

Tendon and ligament injuries are relevant clinical problems in modern society, and the current medical approaches do not guarantee complete recovery of the physiological functionalities. Moreover, they present a non-negligible failure rate after surgery. Failures often occur at the enthesis, which is the area of tendons and ligaments insertion to bones. This area is highly anisotropic and composed of four distinct zones: tendon or ligament, non-mineralized fibrocartilage, mineralized fibrocartilage, and bone. The organization of these regions provides a gradient in mechanical properties, biochemical composition, cellular phenotype, and extracellular matrix organization. Tissue engineering represents an alternative to traditional medical approaches. This work presents a novel biofabrication approach for engineering the enthesis. Gradient-based scaffolds were fabricated by exploiting the combination of electrospinning and three-dimensional (3D) bioprinting technologies. Studies were conducted to evaluate scaffold biocompatibility by seeding bone marrow-derived mesenchymal stem cells (BM-MSCs). Then, the scaffold's ability to promote cellular adhesion, growth, proliferation, and differentiation in both tenogenic and osteogenic phenotypes was evaluated. Fabricated scaffolds were also morphologically and mechanically characterized, showing optimal properties comparable to literature data. The versatility and potentiality of this novel biofabrication approach were demonstrated by fabricating clinical-size 3D enthesis scaffolds. The mechanical characterization highlighted their behavior during a tensile test was comparable to tendons and ligaments *in vivo*.

Keywords: Enthesis; Multiscale and multimaterial 3D bioprinting; Electrospinning; Gradient scaffold; Human mesenchymal stem cells

[†]These authors contributed equally to this work.

***Corresponding author:**
Giovanni Vozzi
(giovanni.vozzi@unipi.it)

Citation: Micalizzi S, Russo L, Giacomelli C, *et al*., 2023, Multimaterial and multiscale scaffold for engineering enthesis organ. *Int J Bioprint,* 9(5): 763. https://doi.org/10.18063/ijb.763

Received: February 19, 2023
Accepted: April 24, 2023
Published Online: May 29, 2023

1. Introduction

The musculoskeletal system plays a key role in maintaining the stability of the human body, providing shape and support during locomotion. It is composed of two main systems: (i) the muscular system, including muscles attached to bones through tendons, and (ii) the

skeletal system, in which bones articulate with each other forming joints whose stability and function are supported by ligaments. Both tendons and ligaments (T/Ls) connect to bones through the osteotendinous junction, also called enthesis. This interface area is crucial for the structural integrity and functionality of the entire musculoskeletal apparatus. The enthesis is a specialized region that facilitates load transmission between dissimilar tissues with a large mismatch in constitutive behavior, such as bone and T/Ls. Depending on the anatomical location, entheses appear either as fibrous or fibrocartilaginous, showing different structural and mechanical properties[1]. In fibrous insertions, T/Ls attach directly to bones with a 45 degrees angle of incidence[2,3]. Fibrocartilaginous entheses are more complex and more relevant from the clinical point of view. They comprise four adjacent tissues that create gradients in topology, mechanical, physiological behavior, and cellular type: (i) T/Ls, (ii) unmineralized fibrocartilage (UFC), (iii) mineralized fibrocartilage (MFC), and (iv) bone. The T/Ls structure is characterized by aligned collagen type I fibrils arranged to form fibers, fascicles, and fibroblasts that synthesize the fibrous collagen-based matrix. Moving into the UFC region, the alignment of the fibers decreases until reaching the MFC region, mainly composed of randomly oriented collagen fibrils (types I, II, and III). Fibroblasts are replaced by fibrochondrocytes that synthesize the extracellular matrix of fibrocartilage, giving the enthesis the ability to withstand compressive loads[4]. The physiological line that separates UFC from MFC is named tidemark. The last zone is bone, where the structure becomes highly hierarchical and populated by osteocytes[5]. Due to this complexity constrained in its micrometer size[6], researchers consider this interface an organ[7]. In modern society, musculoskeletal diseases are the leading cause of disability worldwide, and T/L injuries are the most common[8], where the injury or rupture of a tendon or ligament often occurs at the enthesis. To date, surgical approaches are unable to completely repair a damaged enthesis, registering an increasing number of failures after surgery. In light of this, tissue engineering (TE) provides an alternative to traditional medical approaches. The additive manufacturing technologies in TE allow complex three-dimensional (3D) structures to be fabricated layer-by-layer using biomaterials synthetized *ad-hoc* to replicate features of the targeted tissues. In recent years, the study of interface tissues has become crucial in TE. Several works have been reported in the literature that gradient scaffolds were successfully fabricated to mimic enthesis characteristics. Nowlin *et al.*[9] exploited the electrospinning technology using a collector made of two aluminum bars separated by an air gap. Researchers were able to fabricate a gradient scaffold made of polycaprolactone (PCL) with aligned fibers in the middle and randomly oriented ones externally. Xie *et al.*[10] followed a similar approach to provide a volumetric 3D distribution of the graded tissue. After electrospun-aligned PCL nanofibers on a gap collector, mats were relocated to a planar collector, and random PCL fibers were electrospun on top, obtaining a bilayer construct. A different fabrication approach was used by Xiong *et al.*[11], fabricating a PCL-made gradient scaffold by melt electrowriting (MEW) technology. It is composed of a grid structure with decreasing porosity along the length of the scaffold that mimics the morphological gradient that occurs moving from the bone to the UFC and MFC regions. The scaffold ends with PCL-aligned fibers that mimic the anisotropic orientation of collagen fibers. However, these fabrication approaches are limited to processing only one material with one technology. To fabricate more bioinspired enthesis-like scaffolds, a multitechnological and multimaterial approach is crucial. In this context, Criscenti *et al.*[12] fabricated a multiscale and multimaterial triphasic scaffold by exploiting the combination of fused deposition modeling (FDM) and electrospinning technologies. The scaffold consists of PCL processed by FDM and poly(lactic-co-glycolic acid) (PLGA) processed by electrospinning to replicate the characteristics of bone and T/Ls, respectively. The overlap of the two materials mimics the gradient of the enthesis.

Given the complex 3D structure of T/L and the necessity to scale these scaffolds up to clinically relevant, researchers have investigated the fabrication of twisted, braided, or knitted scaffolds[13]. Barber *et al.*[14] observed enhanced mechanical properties as the braided bundles increased. They fabricated a nanofibrous braided scaffold composed of poly(L-lactic acid) (PLLA) electrospun mats. Sahoo *et al.*[15] developed a biodegradable scaffold fabricated by electrospinning PLGA nanofibers onto a knitted PLGA construct. Exploiting the same technique, Jayasree *et al.*[16] fabricated a braided multiscale fibrous Achilles tendon scaffold consisting of aligned PCL micro/collagen-bFGF nanofibers that showed tendon tissue regeneration *in vivo* after 12 weeks of implantation. However, all these scaffolds lack the proper connection between the T/L and the bone. The other pivotal player in enthesis engineering is cells[10].

Several types of cells have been integrated with the 3D scaffolds in TE. Recently, induced pluripotent stem cells (iPSCs) have been proposed[17]. However, the use of iPSCs still faces several challenges, and mesenchymal stem cells (MSCs) remain the main source of cells in musculoskeletal TE and regenerative medicine[18]. MSCs are stem/stromal cells with self-renewal and multilineage differentiation abilities[19]. They are derived from different tissues. Among these, the adipose-derived (AD-MSCs) and bone marrow-derived (BM-MSCs) MSCs have been mainly used in tendon regeneration. The challenge to recreate a

multiphasic scaffold for enthesis healing has been faced in two main approaches: (i) the direct use of stem cells (i.e., BM-MSCs), or (ii) the use of differentiated cells such as tenocytes, tendon fibroblasts, chondrocytes, and osteoblasts (OBs)[20]. The accessibility of MSCs prompts their choice; however, it requires the development of a scaffold with regional biochemical or mechanical cues to induce specific lineage differentiation in distinct zones[12,17]. In this context, this work aims to design and fabricate an innovative multimaterial and multiscale scaffold capable of inducing cells into a graded enthesis-like tissue comprising a T/L region and a bone region. Specific fabrication methods for different biomaterials were used to obtain the enthesis scaffold. MSCs or pre-committed MSCs into tenocytes and osteoblast were combined within the multiphasic scaffold. With the aim to push forward the T/L engineering, a clinically relevant construct fabricated by braiding three enthesis scaffolds was also presented and characterized.

2. Materials and methods

2.1. Materials

Extensive screening of commercial, medical-grade, and bioresorbable natural and synthetic polymers was conducted to select the most valuable polymers for T/Ls and enthesis engineering. The following materials were evaluated: (i) gelatin from porcine skin (Type A)[21] and (ii) gelatin methacryloyl (GelMA)[22] as natural polymers, (iii) poly(l-lactic acid) (PLLA)[23], (iv) PCL, and (v) 75:25 PLGA as synthetic polymers[12]. Gelatin (gel strength 300, Type A) and PCL (Mn 80,000) were purchased from Sigma-Aldrich (St. Louis, Missouri, United States). GelMA was produced accordingly to the Chen *et al.* protocol[24]. PLLA and PLGA were purchased from Lactel (USA). Solutions were prepared by a solvent casting technique to fabricate scaffolds suitable for cell culture testing. Gelatin solution (10% w/v) was prepared by following the protocol of Pulidori *et al.*[25]. Briefly, the gelatin powder was dissolved in a solution of acetic acid (puriss. p.a., ACS reagent, reag. ISO, reag. Ph. Eur., ≥99.8% from Sigma-Aldrich) and deionized water (DIW) at a ratio of 9:1 and stirred at room temperature overnight. After gelatin dissolution, the 3-(Glycidyloxypropyl) trimethoxysilane (GPTMS) (Sigma-Aldrich) was added as a crosslinking agent. GelMA solution (10% w/v) was prepared following Nichol *et al.*[26] protocol by dissolving it in a 1X Phosphate-Buffered Saline (PBS) solution. Then, 2-Hydroxy-4′-(2-hydroxyethoxy)-2-methylpropiophenone (98% from Sigma-Aldrich, St. Louis, Missouri, United States) (0.5% w/v) was added as a photoinitiator. The GelMA solution was then cured under UV-A (365 nm) light for 30 min. Solutions of PLLA and PLGA (10% w/v) were prepared by dissolving the polymers in chloroform (Sigma-Aldrich, St. Louis, Missouri, United States), while PCL (23% w/v) was dissolved in acetic acid. Scaffolds were fabricated by casting the prepared solutions into Petri dishes at room temperature until solvent evaporation to perform the biological validation.

Table 1. Slicing and printing parameters.

Parameters	Settings	Unit
Infill	50	%
Layer thickness	0.2	mm
Printing speed	12	mm/s
Printing pattern*	Rectilinear	–
Extrusion width	0.4	mm
Nozzle diameter	0.4	mm
Nozzle temperature	160	°C
Bed temperature	35	°C

*Each layer is 90 degrees oriented with the previous one.

2.2. Biofabrication of enthesis scaffold

This section is divided into three sub-paragraphs to explain better the optimization of the fabrication parameters and how the two different technologies were combined to fabricate the enthesis scaffold. As a result of the polymer screening (see results section), the PCL and the PLGA were selected to replicate the bone and T/Ls tissues characteristics, respectively.

2.2.1. Bone-like region

The PCL was processed using the FDM technology to fabricate the scaffold region that would mimic the characteristics of bone tissue. Pellets of medical-grade PCL were used to fabricate filaments suitable for FDM applications through the hot melt extrusion (HME) technology[27]. For this task, a Felfil Evo extruder (Felfil, Turin, Italy) with an extrusion temperature of 100°C, a screw speed of 4 RPM, and an extrusion die of 1.75 mm in diameter was used. A water-cooling element was added to the already implemented air-cooling system to rapidly lower the polymer temperature once extruded and avoid the molten PCL sticky behavior. The extrusion process was performed at room temperature, T = 25°C, and relative humidity, RH, = 35%. The extruded PCL-based filament (final diameter 1.67 ± 0.1 mm) was used to 3D print circular-shaped woodpile grids for cell culture into a 24-multiwell plate (diameter Ø = 13 mm and thickness h = 1 mm) and was suitable for bone tissue engineering applications[28]. Scaffolds were fabricated using a Geeetech A10M 3D printer from Geeetech® (Shenzhen, China). The slicing and printing parameters are listed in Table 1.

2.2.2. Tendon/Ligament-like region

To mimic the physiological, morphological, and mechanical characteristics of T/Ls, a scaffold must exhibit an anisotropic fiber orientation, as in native tissues. In T/Ls, collagen fibers are oriented along the applied stress direction[29]. To replicate this characteristic, PLGA was processed by electrospinning technology. For this application, using and manipulating a strong electric field allow the nanofibers to be extruded and collected in an adjustable manner. To collect aligned fibers, a rotating drum collector was used (drum diameter = 10 cm). PLGA nanofibers were obtained by electrospinning a solution of 10% (w/v) of PLGA dissolved in 1,1,1,3,3,3-hexafluoro-2-propanol (HFIP). This solvent possesses a dielectric constant almost 4 times higher than chloroform allowing thinner fibers to be electrospun[30]. The electrospinning process was performed using a Linari Engineering apparatus (Linari Eng, Italy) featuring a commercial 10 mL syringe with a 21 G needle as its spinneret. Electrospinning parameters were as follows: the applied voltage was 35 kV, the distance between the spinneret and the grounded collector was 10 cm, the rotating speed of the collector was 800 RPM, and the flow rate was 1 mL/h. The process was conducted for 2 h at room temperature, T = 21°C, and relative humidity, RH, = 45%. Samples of electrospun PLGA for cell culture into a 24-multiwell plate were prepared by die cutting.

2.2.3. Enthesis scaffold

The enthesis gradient in physical properties was replicated by developing an *ad-hoc* biofabrication protocol in which PCL was directly 3D-printed on electrospun PLGA mats. Through the 3D printer, two layers of PCL (single layer height 0.2 mm and oriented at 90 degrees to each other) were extruded, fabricating a grid structure on the PLGA strips. The extrusion parameters are the same as listed in Table 1.

2.3. Biological validation of materials

2.3.1. Cell culture

MSCs (human mesenchymal stem cells (bone marrow), SCC034, Millipore, Burlington, Massachusetts, United States) were purchased and were maintained in xeno-free medium (XF MSC expansion medium, cod: SCM045 Millipore, Millipore, Burlington, Massachusetts, United States). Cells were grown at 37°C in 5% CO_2 and detached using Trypsin with EDTA 1x (25-053-CI, Corning Inc., New York, United States) at 80% confluence, used until passage 6.

2.3.2. Mesenchymal stem cells seeding protocol

All the tested scaffolds were sterilized by UV exposure and then washed in phosphate-buffered saline (PBS); moreover, the three synthetic ones were rapidly washed in ethanol (70% in H_2O) before the UV light exposure. After sterilization, scaffolds were incubated overnight in DMEM-F12, supplemented with 10% FBS, 100 U/mL penicillin, and 100 mg/mL streptomycin. On the scaffolds fabricated by solvent casting, the day after the soaking, 20,000 cells were seeded in each well (24-multiwell plate). For the tridimensional scaffolds, 250,000 cells were seeded on 3D-printed PCL in a 24-multiwell plate; 30,000 cells were seeded on an electrospun PLGA scaffold in a 24-multiwell plate. Similarly, for the multimaterial enthesis structure, 30,000 cells were seeded on the PLGA side and 70,000 cells on the PCL side and used for further experiments. As a control, 30,000 cells were seeded on plastic in a 24-multiwell plate.

2.3.3. Viability tests

The MTS assay (CellTiter 96 Aqueous One Solution Cell Proliferation Assay kit, Promega, Madison, Wisconsin, United States) was performed on cells seeded on the scaffolds fabricated by solvent casting in DMEM-F12, supplemented with 10% FBS, 100 U/mL penicillin, and 100 mg/mL streptomycin, after 3 and 7 days of culture, as described by the manufacturer. Briefly, 250 µL of fresh medium was added to each well with 37.5 µL of the MTS reagent and incubated for 2 h at 37°C in 5% CO_2. The supernatants were transferred in a 96-multiwell plate to avoid the interference of the materials, and the absorbance was read at 490 nm (Ensight, PerkinElmer, Waltham, Massachusetts, United States).

2.3.4. Immunofluorescence analysis

Cells were seeded on the scaffolds fabricated by solvent casting (or on the glass as control) and maintained in DMEM-F12, supplemented with 10% FBS, 100 U/mL penicillin, and 100 mg/mL streptomycin for 3 days. Then cells were fixed in 4% paraformaldehyde (PFA) for 15 min, rinsed three times in PBS, permeabilized in PBS-BSA 2.5% with Triton X-100 0.1% for 7 min, and washed and incubated in the blocking solution (PBS-BSA 2.5%) for 1 h at room temperature. Then, samples were incubated with primary antibody Anti-CD90 (HPA003733, Sigma-Aldrich, St. Louis, Missouri, United States) and Anti-Actin (MAB1501, Millipore, Burlington, Massachusetts, United States) diluted in blocking solution overnight at 4°C. The day after, samples were rinsed in PBS-BSA 2.5% and incubated with the secondary antibody (Anti-Rabbit Alexa Fluor 488, A-11001, and Anti-Mouse Alexa Fluor 594, 1:500, A-11012, Thermo Fisher Scientific, Waltham, Massachusetts, United States) for 45 min at room temperature. Finally, cells were rinsed in PBS and mounted with the Fluoroshield mounting medium with DAPI staining (F6057, Sigma Aldrich, St. Louis, Missouri, United States), and images were acquired using a Nikon E-Ri microscope with a magnification of 60x.

Figure 1. (A) Typical setup for the tensile testing of the enthesis scaffolds, and (B) setup of the DIC model through the Ncorr tool. The black markers were manually drawn onto the surface scaffold to better perform the DIC analysis.

2.4. Morphological characterization

The morphology of the enthesis scaffolds was characterized from its nano- to macroscale, and its features were then compared with those of the tissues constituting the enthesis organ. The nanostructure of the enthesis scaffold was studied by scanning electron microscopy (SEM) imaging analysis (Quanta 450 FEG microscope, FEI, Hillsboro, Oregon, USA). The images acquired by SEM were analyzed by ImageJ software using the DiameterJ plug-in. Pore area, fiber diameter, and fiber orientation were evaluated. The PLGA fiber integrity at the mixed region level, after the PCL extrusion process, was also evaluated. The study was conducted by analyzing samples in triplicate.

2.5. Mechanical characterization

The enthesis scaffold is a multimaterial construct composed of two structures processed through different technologies and joined together. The interface region can represent a critical point from the mechanical point of view and must be deeply investigated. The mechanical characterization was carried out by performing uniaxial tensile tests using a universal machine Zwick-Roell Z005 ProLine equipped with a 100 N load cell. Rectangular-shaped specimens, with a length-to-width ratio of 4:1 (length 20 ± 0.15 mm and width 5 ± 0.3 mm), were tested in triplicate until failure by setting a strain rate of 10%/min of the initial length. The tensile tests were video recorded to perform a Digital Image Correlation (DIC) analysis to investigate the behavior of each region of the enthesis scaffold[31,32]. The DIC analysis was performed by using the Ncorr tool of MATLAB® software. Figure 1 shows the tensile test setup and markers applied for each scaffold region for DIC analysis. The DIC tool allows the displacement field of the tested specimens to be mapped and evaluated. The stress–strain curves were used to calculate the following parameters: Young's modulus E (MPa), ultimate stress σ_{max} (MPa), ultimate strain ε_{max} (%), and toughness U (J/m^3). The specimen failure modality was also considered.

2.6. Biological validation of enthesis scaffold

2.6.1. Osteoblast differentiation and alizarin red staining

MSCs were seeded on the 3D-printed PCL region of the enthesis scaffolds as described above. The osteogenic differentiation was initiated by the replacement of the media with the Osteogenesis Differentiation Medium (StemPro™ A1007201, Thermo Fisher Scientific, Waltham, Massachusetts, United States). The medium was replaced every 3 days, and the mineralization was quantified after 14 days of differentiation. The quantification of osteoblast differentiation was evaluated using alizarin red staining as previously reported[33]. Briefly, scaffolds were washed in PBS, and cells were fixed in 4% PFA solution for 20 min. In the end, the scaffolds were washed three more times with PBS. Alizarin red staining was performed by dipping scaffolds in the alizarin staining solution (TMS-008, Millipore, Burlington, Massachusetts, United States) for 1 h. In the end, the scaffolds were washed three times with PBS, and then the absorbance was read at 550 nm (Ensight, PerkinElmer, Waltham, Massachusetts, United States) by dissolving the dye in a cetylpyridinium chloride solution. Pre-differentiated cells were also used with the enthesis scaffold. Specifically, cells were differentiated for 3 days as described above, seeded on the scaffold or plastic for further 14 days, and maintained in a growth medium for the experiment.

2.6.2. Tenogenic differentiation and aniline blue staining

MSCs were seeded on the electrospun PLGA region of the enthesis scaffolds as described above. The tenogenic

differentiation was initiated by the replacement of the media with tenogenic differentiation medium (DMEM-F12 supplemented with 5% FBS, 1% penicillin/streptomycin, 100 ng/mL CTGF, 50 μg/mL ascorbic acid, 100 ng/mL BMP-12, and 50 ng/mL TGF-β3). The medium was replaced every 3 days for 21 days. The aniline blue staining was used to quantify the collagen deposition. Aniline blue staining was performed using the trichrome staining kit (HT15, Sigma-Aldrich, St. Louis, Missouri, United States) following the manufacturer's instructions. Briefly, cells were treated with a phosphomolybdic/phosphotungstic acid solution at a ratio of 1:1, stained with the dye, and fixed with an acetic acid solution, and the dye was extracted from the cells using DMSO. Absorbance was read at 670 nm (Ensight, PerkinElmer, Waltham, Massachusetts, United States). Pre-differentiated cells were also used with the enthesis scaffold. Specifically, cells were differentiated into tenocytes for 7 days, as described above, then seeded on the scaffold or plastic for further 21 days and maintained in a growth medium for the experiment.

2.7. Fabrication of clinically-relevant scale scaffold

Three enthesis scaffolds were manually braided to fabricate a clinical-scale scaffold and demonstrate the versatility and potentiality of scaling up this novel biofabrication approach. In this sense, scaffolds should replicate the T/Ls *in vivo* morphology, structure, and size, but they should also present a region that optimizes insertion into the bone and reduces the risk of failure after surgery. These clinically-relevant scale scaffolds were mechanically characterized by performing the same uniaxial tensile tests conducted for the enthesis scaffolds. The elastic modulus was calculated by introducing the packing factor (PF)[34]. This parameter considers the air gaps that form during the braiding process. The PF is defined as follows:

$$\mathrm{PF} = n \cdot \frac{A_s}{A_b} \quad \text{(I)}$$

where n is the number of enthesis scaffolds used in the braiding process, and A_s and A_b are the cross-sections of the single enthesis scaffold specimen and the braided scaffold approximated with a cylindrical shape, respectively. The PF is used to calculate the effective elastic modulus E_b of the 3D braided scaffolds with the following relationship:

$$E_b = \frac{E}{\mathrm{PF}} \quad \text{(II)}$$

where E is the elastic modulus calculated from the stress–strain curve without considering air gaps. At this stage, no biological tests were conducted. Scaffolds were only mechanically characterized.

2.8. Statistical analyses

Statistical analyses were performed using Prism 8 software version 8.2.1 (GraphPad software, United States). Data were analyzed using one-way ANOVA followed by Sidak multiple comparisons *post hoc* test. All data are expressed as means ± standard deviation (SD), and a p value of 0.05 was considered significant for all experiments.

3. Results and discussions

3.1. Polymers' ability to support MSC adhesion and growth

Scaffolds fabricated by solvent casting (N = 30 per polymer type, diameter Ø = 13 mm, and thickness h = 0.5 ± 0.1 mm) were biologically tested. Additional information can be found in **Figure S1** (Supplementary File). The results of the biocompatibility tests are shown in Figure 2. MSCs' ability to adhere and grow on different types of solvent-casting scaffolds was first evaluated using the MTS assay (Figure 2A and B). MSCs were seeded on polymers or plastic culture plates (CTRL) and maintained in a growth medium for 3 or 7 days. Results demonstrated the ability of all the tested solvent-casting scaffolds to sustain the MSC adhesion after 3 (Figure 2A) and 7 (Figure 2B) days. All the constructs showed an average of five times lower number of adherent cells with respect to CTRL. However, they were all able to sustain the MSC growth rate, as evidenced by the lack of difference in the percentage of cell proliferation after 3 or 7 days of culture with respect to CTRL. The PLGA ones demonstrated the best ability to promote MSC adhesion and growth among all the scaffolds. Based on these results and literature data[35,36], PLGA and PCL were selected for other experiments. The ability of MSCs to adhere to PLGA and PCL solvent-casting scaffolds was further investigated by immunofluorescence analysis (Figure 1C). MSCs were seeded on scaffolds (or glass as control) and maintained in a growth medium for 3 days; at the end, cells were stained with anti-CD90 (red) as a marker of MSCs[37] and anti-actin (green) as a marker of cytoskeleton organization. Both PLGA and PCL were able to support the MSC adhesion, in accordance with the MTS results. Interestingly, the two solvent-casting polymers differently modified the MSC cytoskeleton organization. Cells grown on PLGA displayed overall cell elongation and parallel cytoskeletal conformation, as evidenced during the MSC differentiation to tenocytes[38]. Conversely, several studies have reported that MSCs exhibit a star shape during osteogenic lineage commitment[39,40]. In this respect, as evidenced by immunofluorescence images, PCL mainly supported star shape actin organization. These results prompted us

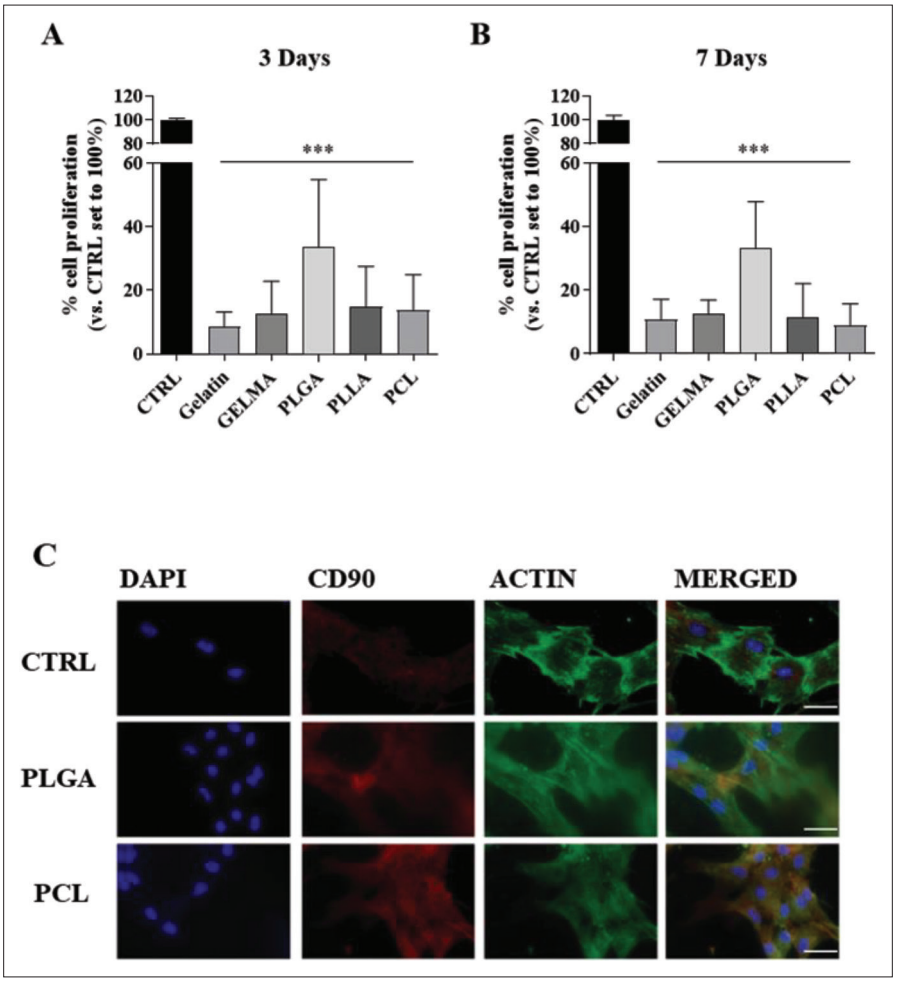

Figure 2. (A) Evaluation of solvent casting scaffolds biocompatibility. MSCs were seeded on different scaffolds for 3 (A) or 7 (B) days. In the end, the MTS assay was performed. Data are expressed as the percentage of cell proliferation versus MSCs seeded on plastic as control (CTRL) and represent the mean ± SD of three independent experiments. ***$p < 0.001$ vs. CTRL (C) Representative images of MSCs adhesion on glass (CTRL), PLGA, or PCL. DAPI (blue), CD90 (red), and actin (green). Scale bar = 50 μm.

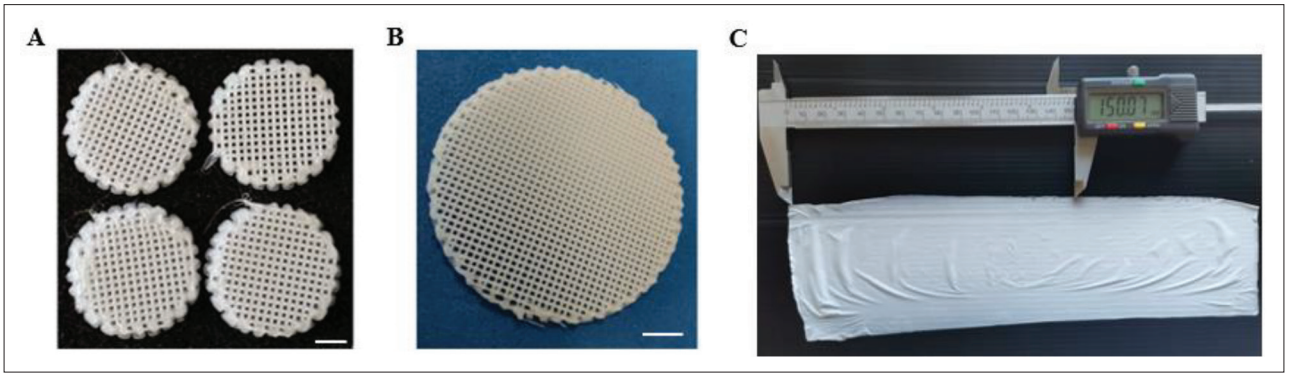

Figure 3. (A) 3D-printed PCL bone-like scaffold suitable for cell culture in a 24-well plate (scale bar length = 3 mm) and (B) 6-well plate (scale bar length = 5 mm). (C) PLGA-made non-woven mats fabricated by electrospun onto the rotating drum collector.

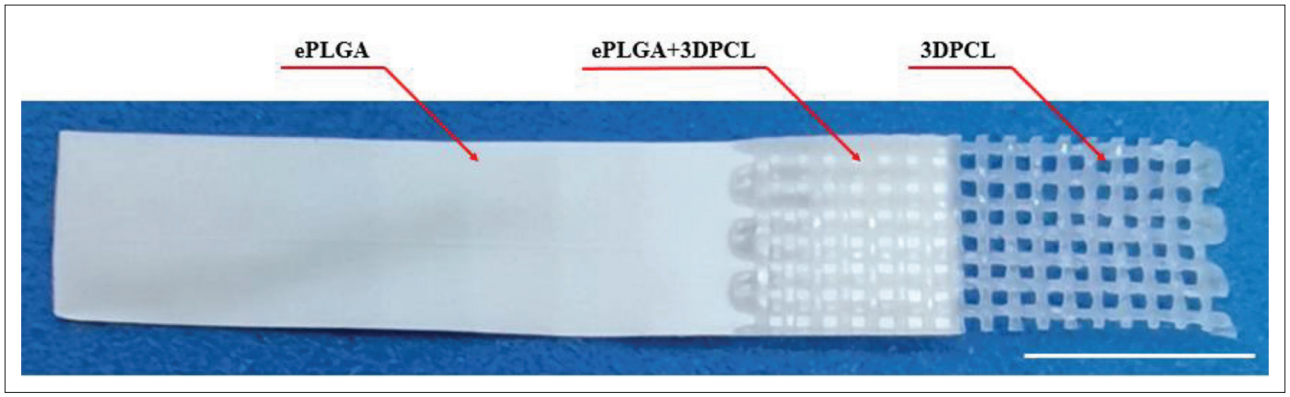

Figure 4. Illustration of the enthesis scaffold. From left to right: (i) region that mimics the T/Ls behavior made of electrospun PLGA (ePLGA), (ii) interface region composed of PCL extruded onto the PLGA structure (ePLGA+3DPCL), and (iii) region that mimics the bone tissue characteristics made of PCL (3DPCL). Scale bar length = 5 mm.

to select PLGA and PCL for tenogenic and osteogenic differentiation, respectively.

3.2. Enthesis scaffold

Before fabricating the enthesis scaffold, the 3D printing and electrospinning processes were optimized (data not shown). Medical-grade PCL-based filaments with a diameter Ø = 1.67 ± 0.50 mm (additional information can be found in **Figure S2** in Supplementary File) were fabricated through the HME technique and used to 3D-printed grid-shaped scaffolds (Figure 3A and B). Additional information about the setup of the 3D printing and electrospinning processes is reported in **Figure S3** (Supplementary File). The two additive manufacturing technologies were combined to fabricate the enthesis scaffold shown in Figure 4.

In Figure 4, three different regions can be identified: (i) a T/Ls-like region made of electrospun PLGA (length L = 15.0 ± 0.10 mm, width W = 5.0 ± 0.10 mm, and thickness h = 175.0 ± 30.00 µm), (ii) a bone-like region made of 3D-printed PCL (length L = 5.0 ± 0.10 mm, width W = 5.0 ± 0.10 mm, and thickness = 0.4 ± 0.02 mm), and (iii) an interface region (length L = 5.0 ± 0.10 mm, width W = 5.0 ± 0.10 mm, and thickness = 0.40 ± 0.05 mm) where the two structures interact to create a multimaterial and multiscale scaffold with gradients in morphological and material properties. The scaffold has length and width in a ratio of 4:1, suitable for tensile tests.

3.3. Morphological characterization

The analysis of the electrospun region highlighted a fiber diameter of 480 ± 200 nm with 42% of fibers with a diameter less than 500 nm. Obtained data are comparable with collagen fibrils in human tendons, which present 20–500 nm in diameter and form a primary bundle of sub-fascicles[41]. Collecting fibers onto a rotating collector at 800 RPM allowed non-woven mats presenting fibers with anisotropy in the fiber orientation to be fabricated. The 60% of fibers presented an orientation in a range of ±20 degrees. More in-depth information is illustrated in Figure 5. Electrospun PLGA fibers (Figure 5D) showed anisotropy orientation, a wavy shape, and both aligned and crossed fibers like collagen fibers in the human tendon[29] (Figure 5A). The PCL-region imaging study revealed a fiber diameter of 440 ± 15 µm and 45% ± 2.5% porosity, in line with the printing parameters listed in Table 1 and the literature data[42]. The interface region imaging confirmed that the two materials interact without interfering with each other. The PLGA fibers were only melted at the line of PCL deposited during the printing process. More details are reported in Figure 6.

3.4. Mechanical characterization

The mechanical behavior of the scaffold was evaluated by performing uniaxial tensile tests. The tensile strength at the interface between the electrospun PLGA and the extruded PCL in the mixed region was the region under the "magnification glass." In all tested specimens, the electrospun area underwent the largest deformation. All specimens failed in the center of the electrospun area, confirming that the mechanical tests were correctly performed and the proper integration between the bone and T/Ls-like regions. Both mixed and PCL regions were stable and able to handle the strain, as shown in Figure 7. The characteristic stress–strain curve of the tested specimens (Figure 7D) shows behavior comparable to the electrospun PLGA structures with aligned fibers[43,44]. This result highlights how this area was the only one that deformed to the point of failure. The PCL-printed and mixed regions did not appear to affect the behavior of the entire structure during the tensile test. This result is confirmed by the DIC analysis. Figure 8 shows the scaffold strain along the *y*-axis during the tensile test.

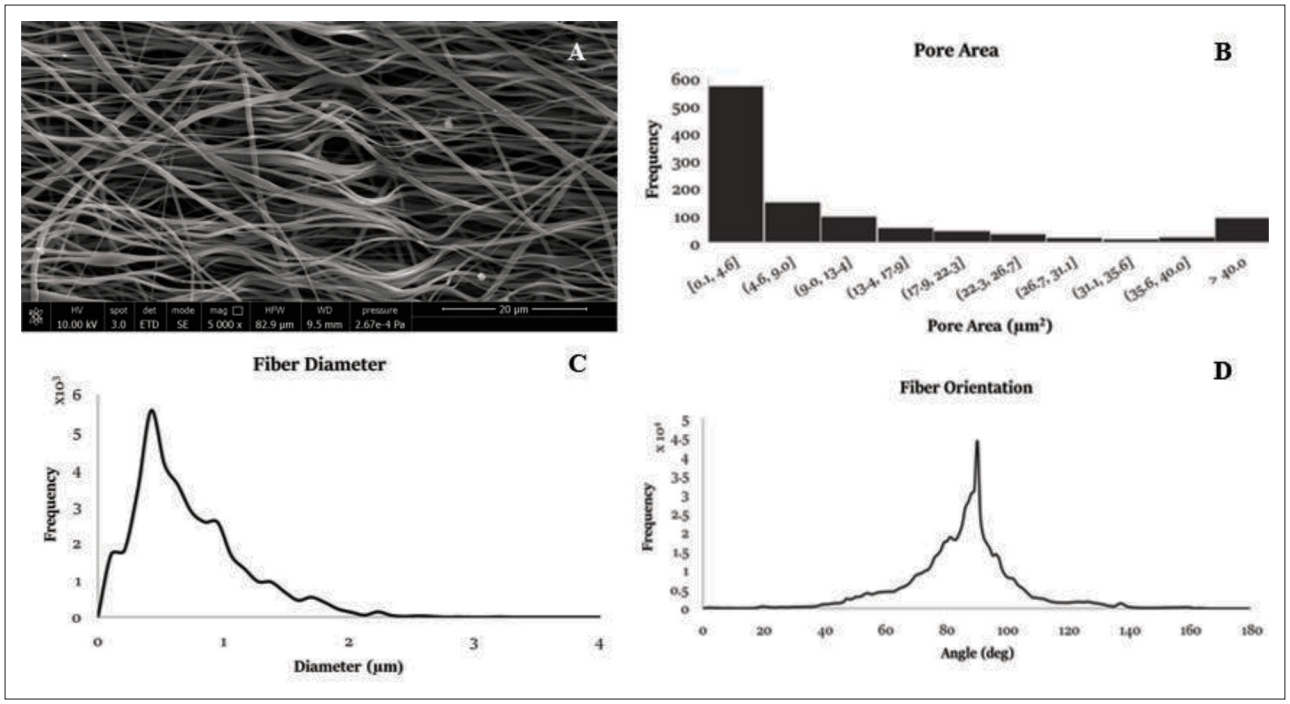

Figure 5. Results of the PLGA scaffold region analysis. (A) SEM image of a sample obtained by electrospun PLGA onto the rotating collector at 800 RPM (SEM parameters: high voltage HV = 10 kV, horizontal field of view HFV = 82.9 μm, magnification mag = 5000x, working distance WD = 9.5 mm, and scale bare length SBL = 20 μm). (B) Pore area distribution histogram (*y*-axis label: frequency, min frequency = 0 and max frequency = 50,000; *x*-axis label: Pore Area (μm²), first pore area range 0.1–4.6 μm² and last pore area range > 40 μm²). (C) Fiber diameter distribution (*y*-axis label: frequency, min frequency = 0, and max frequency = 6000; *x*-axis label: diameter (μm), min diameter = 0 μm, and max diameter = 4 mm). (D) Fiber orientation distribution (*y*-axis label: frequency, min frequency = 0 and max frequency = 50,000; *x*-axis label: angle (deg), min angle = 0 degrees and max angle = 180 degrees).

Figure 9 illustrates the specimen strain along the *x*-axis. The strain modeled by the DIC analysis differs by 3.4% from the value calculated from experimental data. The color map of the strain field along the *y*- (Figure 8) and *x*-axis (Figure 9) shows how along both axes, the only region that deformed was the electrospun PLGA. Therefore, it is possible to assume that the mechanical behavior of the scaffold can be attributed to this region. The mechanical parameters of enthesis scaffolds were E = 530 ± 93 MPa, σ_{max} = 6.0 ± 0.8 MPa, ε_{max} = 70% ± 3%, and $U = 1.3 \pm 0.5 \times 10^6$ J/m³), which are in line with data reported in the literature. The elastic modulus, E, presents a mean value similar to the supraspinatus tendon anterior sub-region[45]. The other parameters are comparable with data reported in the literature regarding electrospun PLGA mats with aligned fibers[46,47]. When comparing data with the literature, the enthesis scaffolds show improved mechanical properties: Balestri *et al.*[48] fabricated an *in vitro* model of a bone–tendon–muscle interface that recorded an elastic modulus of hundreds of kPa; Criscenti *et al.*[12] provided an enthesis scaffold fabricated by electrospun PLGA onto PCL grids registering Young's modulus as less than 100 MPa.

3.5. Biological validation

3.5.1. Osteoblast differentiation support by 3D-printed PCL

MTS assay was first performed to assess the ability of the 3D-printed PCL scaffolds to prompt MSC adhesion and growth (Figure 10A and B) by seeding MSCs on them or plastic culture plates (CTRL) and maintaining in growth medium for 3 or 7 days. Results demonstrated the ability of 3D-printed PCL scaffolds to sustain the MSCs adhesion after 3 (Figure 10A) and 7 (Figure 10B) days, in accordance with the results on solvent-casting scaffolds (Figure 2A and B). It was also able to sustain the MSCs growth rate as evidenced by the lack of difference in the percentage of cell proliferation after 3 or 7 days of culture with respect to the plastic. Then, the ability of the 3D-printed PCL structures to promote and maintain the osteogenic differentiation was evaluated by assessing the mineralized matrix formation on the scaffold (Alizarin red staining; Figure 10C–F). MSCs were seeded on plastic culture plates or 3D-printed PCL, and two protocols were used (Figure 10C): (i) cells were maintained in growth medium (CTRL and 3D-printed PCL samples) or (ii) in osteogenic medium (Osteo and Osteo 3D-printed PCL samples) for 14 or

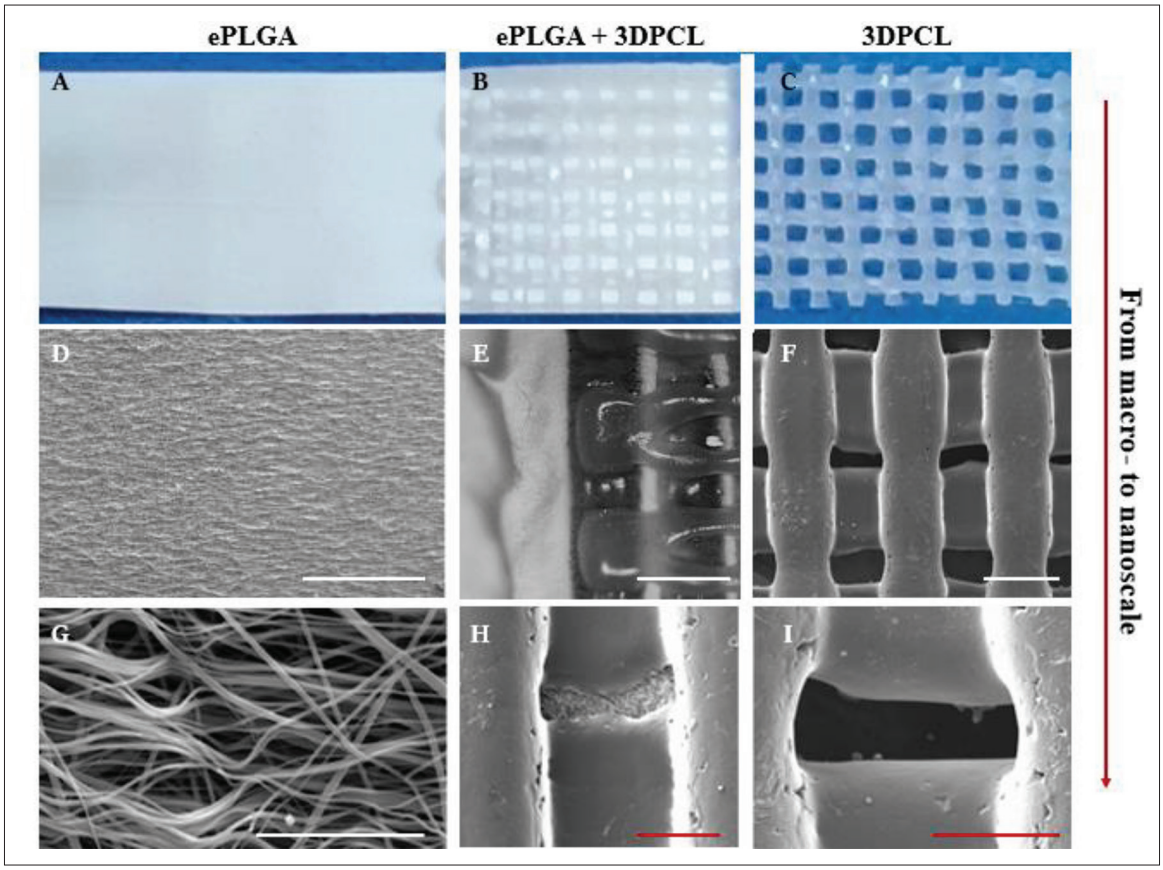

Figure 6. Illustration of the enthesis scaffold from macro- to nano-scale. (A–C) Full-size scaffold regions. (D, F) SEM and (E) optical microscope (20x magnification) images highlighting the microscopic structure. Scale bar length: (D–F) 500 μm. (G–I) SEM images of the scaffold at the micro- and nano-scale. Scale bar lengths: (H, I) 200 μm and (G) 20 μm.

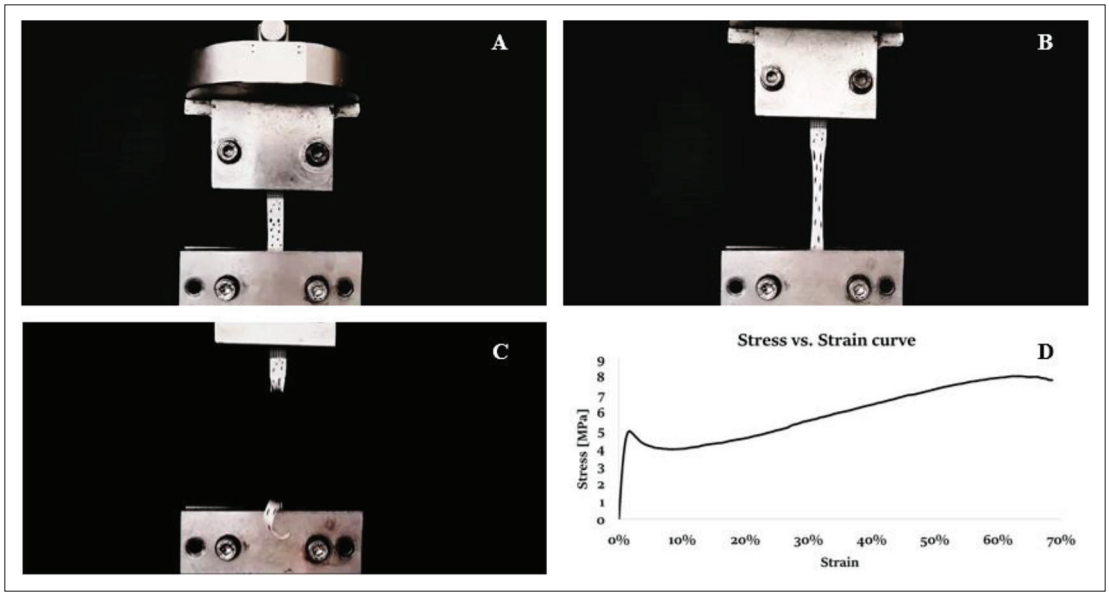

Figure 7. Uniaxial tensile test results. (A–C)Three different moments illustrating a sample of enthesis scaffold during a tensile test. (C) Failure occurs in the central part of the PLGA region. (D) Characteristic stress–strain curve of the enthesis scaffold.

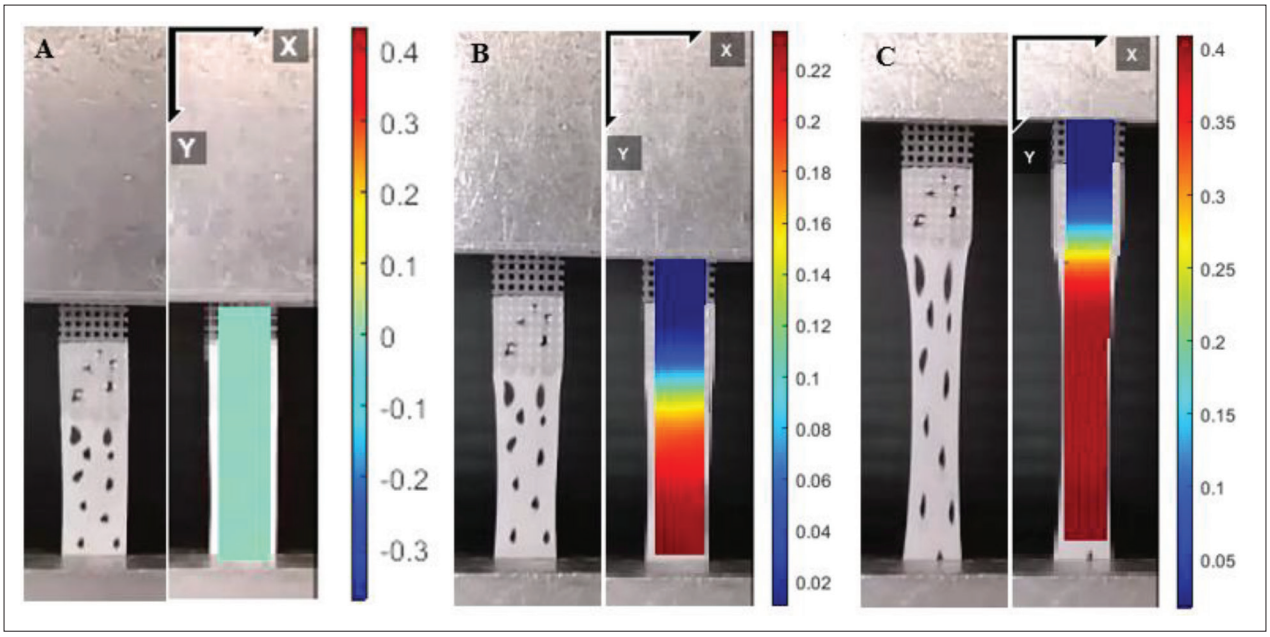

Figure 8. Color map of the strain (blue = minimum value and red = maximum value) along the *y*-axis evaluated at three different time points during the uniaxial tensile test. Minimum and maximum strain values: (A) min = max = 0, (B) min = 0.02 and max = 0.23, and (C) min = 0.03 and max = 0.44.

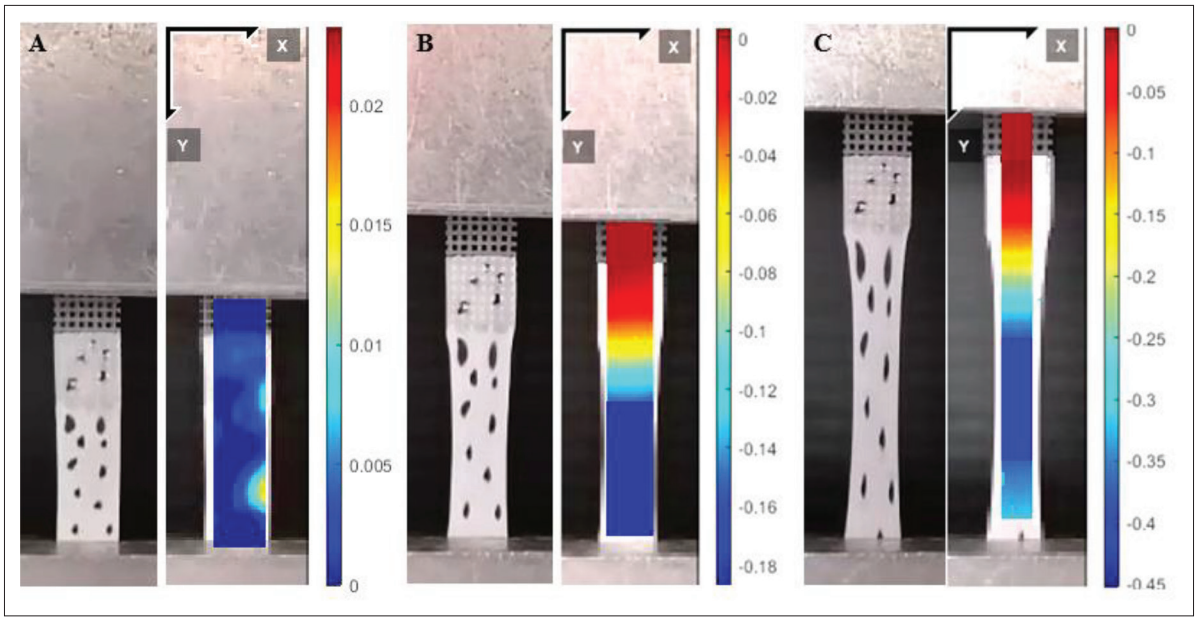

Figure 9. Color map of the strain along the *x*-axis evaluated at three different time points during the uniaxial tensile test. The specimen exhibits a strain along the *x*-axis. Minimum and maximum strain values: (A) min = 0.0144, median = -0.00, and max = -0.0138, (B) min = 0 and max = -0.18, and (C) min = 0 and max = -0.45.

21 days. As expected, a significant difference in calcium accumulation was evidenced in the samples cultured in an osteogenic medium compared to cells maintained in a growth medium. 3D-printed PCL scaffolds *per se* were able to slightly stimulate the calcium deposition when MSCs were maintained in a growth medium for 14 days, and the increase became significant after 21 days of culture (Figure 10E) in accordance with literature data[49]. MSCs grown on the scaffold and maintained in the osteogenic medium were able to significantly increase calcium and phosphate deposits after 14 and 21 days (Figure 10F). The scaffold was not able to support the differentiation process at the same levels of MSCs seeded on plastic (Osteo) after 14 days

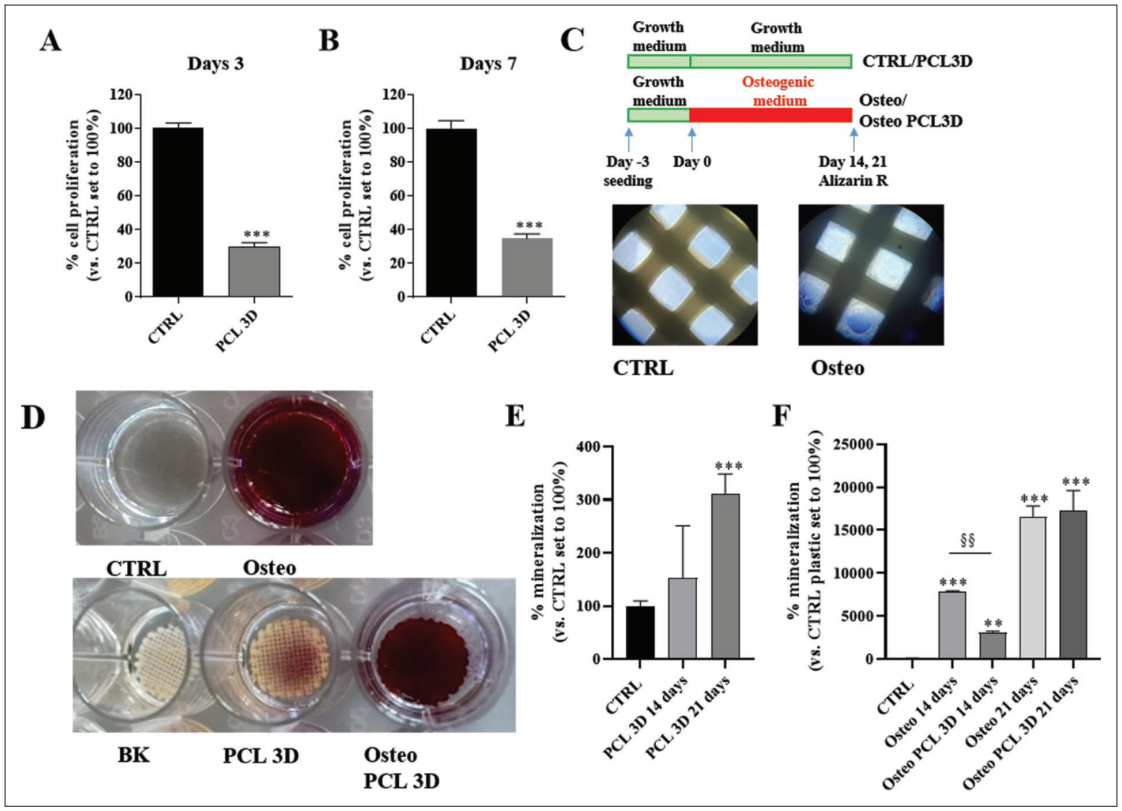

Figure 10. Proliferation and differentiation of MSCs on 3D-printed PCL scaffolds (PCL 3D). MSCs were seeded on different constructs for 3 (A) or 7 (B) days. In the end, the MTS assay was performed. Data are expressed as the percentage of cell proliferation versus undifferentiated MSCs seeded on plastic (CTRL). (C) Schematic representation of differentiation protocol used (up panel). Representative image of the 3D-printed PCL scaffolds after 14 days of osteoblast differentiation (down panel). (D–F) Cells were seeded on the 3D-printed PCL scaffolds (PCL 3D) or on plastic (CTRL) and maintained in a growth medium or differentiating medium (Osteo) for 14 or 21 days. In the end, alizarin red staining was performed, and representative images were reported (D). Data are expressed as the percentage of mineralization versus non-differentiated (CTRL) MSCs grown on plastic. Data are the results of three independent experiments. $^{**}p < 0.01$, $^{***}p < 0.001$ vs. ND; §§ $p < 0.01$ vs. CTRL.

of differentiation, in accordance with the lower number of adherent cells (Figure 10A–B). However, the level of mineralization became comparable after 21 days of differentiation, supporting the use of 3D PCL for the generation of bone-like regions in the enthesis scaffold.

3.5.2. Tenogenic differentiation support by electrospun PLGA

MTS assay was performed to assess the ability of the electrospun PLGA scaffolds to prompt MSC adhesion and growth (Figure 11A and B) by seeding MSCs on them or plastic culture plates (CTRL) and maintaining in growth medium for 3 or 7 days. The electrospun PLGA scaffolds were able to sustain the MSC adhesion after 3 (Figure 11A) and 7 (Figure 11B) days, in accordance with the results on solvent-casting constructs (Figure 2A and B). It was also able to sustain the MSCs growth rate as evidenced by the lack of difference in the percentage of cell proliferation after 3 or 7 days of culture with respect to the plastic. The ability of electrospun PLGA in parallel fibers to promote and maintain the MSC differentiation into tenocytes was evaluated by assessing the amount of collagen deposition on the scaffold (aniline blue staining; Figure 11C–F). As for osteogenic differentiation, MSCs were seeded on plastic culture plates or electrospun PLGA scaffolds (Figure 10C) and were maintained in a growth medium (CTRL and electrospun PLGA samples) or a tenogenic medium (Teno and Teno electrospun PLGA samples) for 14 or 21 days. The amount of collagen deposition was not significantly increased by PLGA scaffolds *per se* after 21 days of culture (Figure 11E). A significant difference in collagen deposition was evident in the samples cultured in a tenogenic differentiation medium compared to cells maintained in a growth medium only after 21 days of culture (Figure 11F). PLGA constructs were able to sustain the tenogenic differentiation of MSCs when the tenogenic medium was applied, reaching similar levels of collagen deposition with respect to cells grown on plastic (Figure 10F), supporting the use of electrospun PLGA for the generation of T/Ls-like region in the enthesis scaffold.

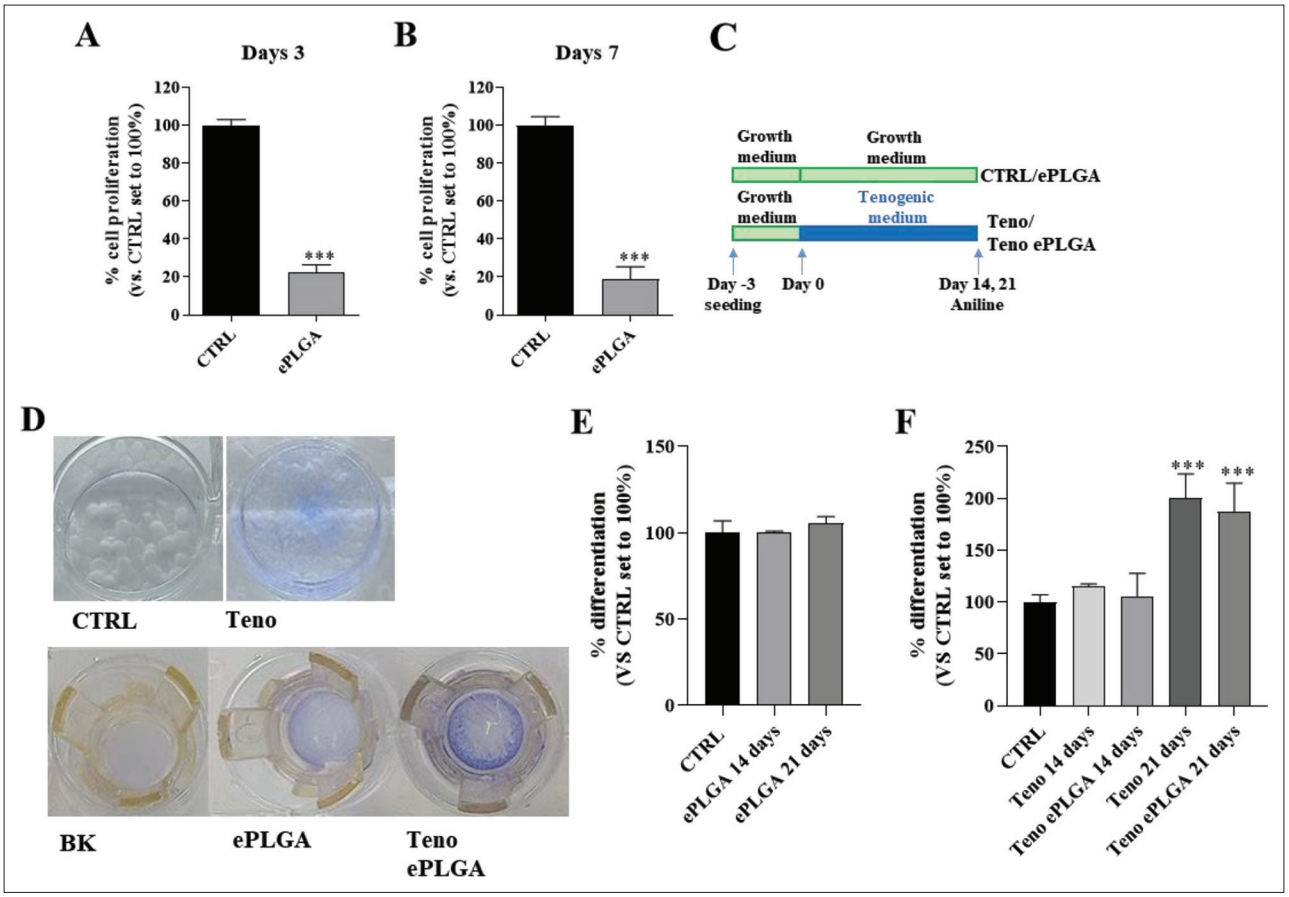

Figure 11. Proliferation and differentiation of MSCs on electrospun PLGA scaffolds (ePLGA). MSCs were seeded on different scaffolds for 3 (A) or 7 (B) days. In the end, the MTS assay was performed. Data are expressed as the percentage of cell proliferation versus undifferentiated MSCs seeded on plastic (CTRL). (C) Schematic representation of differentiation protocol used. (D–F) Cells were seeded on the electrospun PLGA scaffolds (ePLGA) or plastic (CTRL) and maintained in a growth medium or tenogenic medium (Teno) for 14 or 21 days. In the end, aniline blue staining was performed, and representative images after 21 days were reported (D). Data are expressed as the percentage of differentiation versus non-differentiated (CTRL) MSCs grown on plastic. Data are the results of three independent experiments. ***$p < 0.001$ vs. CTRL.

3.5.3. Differentiation of MSC on multimaterial scaffolds

To assess the ability of the enthesis scaffold to promote and maintain both the osteogenic and tenogenic differentiation, alizarin red and aniline blue stainings were performed. Thus, undifferentiated MSCs were seeded on the enthesis scaffold and maintained in a growth medium for 14 and 21 days to assess the ability to support osteoblast and tenocyte differentiation, respectively (Figure 12A). In fact, the calcium deposition was already significantly increased after 14 days of culture on the scaffold (Figure 10E and F). Conversely, 21 days were needed to obtain a significant deposition of collagen (Figure 11E and F). The enthesis scaffold slightly induced osteoblast and tenocyte differentiation when undifferentiated MSCs were used (Figure 12B and C). Then to induce the differentiation, MSCs were primed with osteogenic or tenogenic medium (pre-differentiated MSC) before being seeded on the scaffold. Specifically, osteoblast pre-differentiated cells were seeded on the PCL region and tenocyte pre-differentiated cells on the PLGA region and then maintained in a growth medium. As expected, osteogenic pre-differentiated cells were able to improve their differentiation into osteoblasts on enthesis, with a significant increase of calcium deposition with respect to the undifferentiated ones (Figure 12B). Similarly, tenogenic pre-differentiated cells were able to significantly increase the collagen deposition on enthesis with respect to the undifferentiated ones (Figure 12C).

3.6. Clinically-relevant scale scaffold

Uniaxial tensile testing results of 3D braided scaffolds are shown in Figure 13. Analyzing the stress–strain curve (Figure 13B), it is possible to distinguish: (i) the

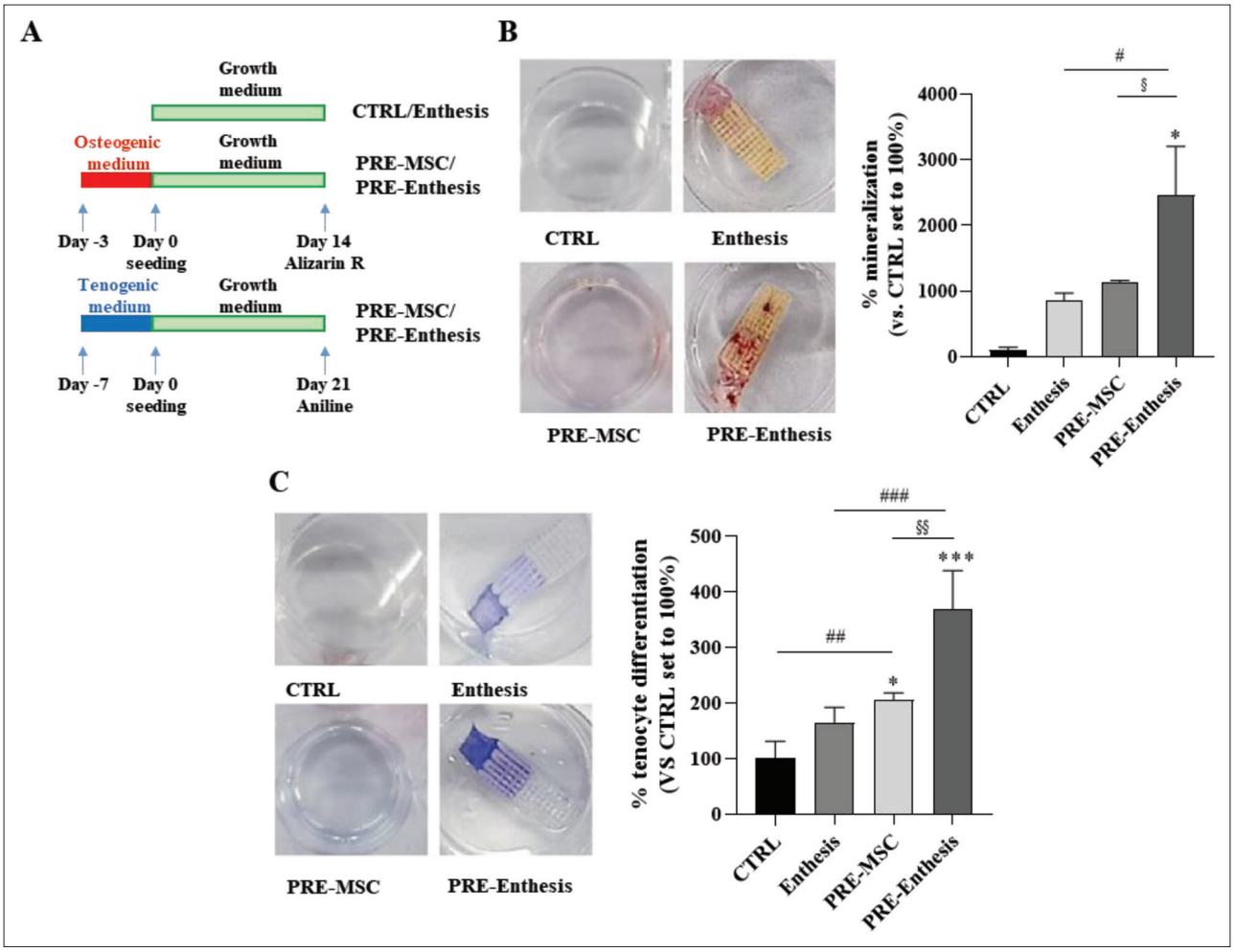

Figure 12. MSCs osteogenic/tenogenic differentiation support by the enthesis scaffold. (A) Schematic representation of protocol used. (B, C) MSCs or pre-differentiated MSCs (PRE-MSC) were seeded on the enthesis scaffold (Enthesis) or plastic (CTRL) and maintained in a growth medium. (B) After 14 days of differentiation, alizarin Red staining was performed. (C) After 21 days of differentiation, aniline blue staining was performed. Representative images were shown. Data are the results of three independent experiments. * $p < 0.05$, ***$p < 0.001$ vs. ND; § $p < 0.05$, §§ $p < 0.01$; # $p < 0.05$, ## $p < 0.01$, ### $p < 0.001$ vs. CTRL.

toe, (ii) the linear, and (iii) the yield regions[45]. The stress slowly increases with strain within the toe region (0%–7% strain). This non-linear behavior can be related to the braided structure. During the initial phase of loading, the fiber bundles start to align from a wavy shape. They elongate according to the direction of the applied uniaxial force. The force is progressively transmitted to the interconnected fiber bundles and their component nanofibers, resulting in linear mechanical behavior with a constant elastic modulus in the linear region (7%–12% strain). As the applied stress increases, the yield region is reached, extending the strain from 13% to approximately 65%. At this stage, the woven fiber bundles reached maximum alignment, starting to deform plastically until failure. The mechanical parameters of braided scaffolds are as follows: E = 235 ± 15 MPa, σ_{max} = 8 ± 0.25 MPa, ε_{max} = 65% ± 12%, and U = 1.03 ± 0.25 × 10^6 J/m^3. These data are in line with the literatures. As reported in the work of Ramakrishna *et al.*[50], researchers fabricated electrospun braided scaffolds made of poly(lactic acid) (PLA) with Young's modulus of in a range of 300–800 MPa. Mechanical parameters are also comparable to the *in vivo* tissues such as the Achilles Tendon (AT), which are presented as E = 266 ± 106 MPa and ε_{max} = 48% ± 15%. The ultimate stress of the AT remains significantly higher, with a value of 47 ± 17 MPa, as reported in the study by Brennan *et al.*[45]. In addition, the fabricated clinically-relevant scaffolds have the unique characteristic of being triphasic, while braided scaffolds in the literature present a single phase.

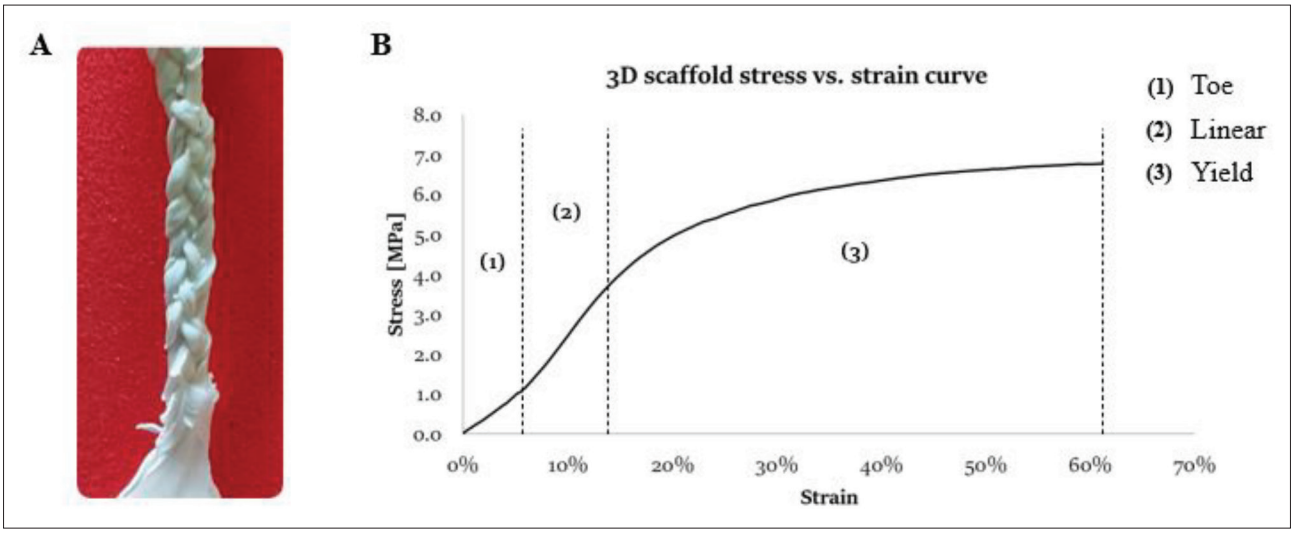

Figure 13. (A) 3D scaffold fabricated by braiding $n = 3$ enthesis structures and (B) characteristic stress–strain curve.

4. Conclusion

Enthesis engineering requires a multiscale and multimaterial biofabrication approach in order to fabricate scaffolds that exhibit physicochemical characteristics of both soft and hard tissues. Current fabrication technologies must be updated to replicate such complex tissues. Extrusion-based bioprinting, for example, lacks recreating the nanostructure of *in vivo* tissues. The electrospinning technology can replicate the micro- and nanostructure of human tissues, but it cannot be used to fabricate constructs with complex geometries. The simultaneous or combined processing of multiple materials to obtain graded scaffolds is a challenge. The presented approach aims at overcoming these limitations by exploiting the combination of different additive manufacturing technologies. To this purpose, a novel biofabrication protocol that exploits the combination of 3D printing and electrospinning technologies was developed. At first, the most valuable polymers for this application were selected. Among all the tested materials, PLGA and PCL showed a better ability to promote MSCs adhesion, proliferation, and differentiation. PLGA showed the ability to induce tenogenic differentiation of MSCs, while the PLC differently affected actin fiber organization, as evidenced by immunofluorescent staining, supporting the ability to induce osteogenic differentiation of MSCs. The enthesis scaffold was fabricated by 3D printing a PCL grid onto the electrospun PLGA surface. It presented three regions with different morphological, mechanical, and chemical characteristics. Constructs showed optimal morphological properties and enhanced mechanical behavior comparing to the literature data. The interface between the two materials was able to support the strain during the tensile test. The enthesis scaffold also demonstrated the ability to support MSC adhesion and differentiation in both osteoblasts and tenocytes, supporting its development as a tool for regenerative medicine in enthesis engineering. Future lines of research should investigate the effects of mechanical stimulations on cell growth and differentiation. Although bioreactors able to impose well-controlled physical and chemical stimuli have been described[51–53], the connection between the scaffolds and the anchoring system is usually not straightforward. Furthermore, the stimulation protocol should be carefully tuned. In order to demonstrate the versatility of this biofabrication approach, clinically relevant scaffolds that showed optimal mechanical behavior comparable with *in vivo* tendons and ligaments were fabricated by manually braiding three enthesis scaffolds. Braided scaffolds reported in the literature well replicated T/L characteristics but were made of bundles of the same material. They also did not present the enthesis region to optimize the insertion to the bone, which was achieved with interference screws. On the contrary, we presented a scaffold with a graded area typical of the enthesis organ, featuring both T/L and bone regions, envisioning a possible clinical scale-up.

Acknowledgments

The authors acknowledge the support of the Crosslab Additive Manufacturing of the Department of Information Engineering, University of Pisa.

Funding

This research work is supported by the "TRITONE project" founded by "Regione Toscana" with "BANDO RICERCA SALUTE 2018."

Conflict of interest

The authors declare no conflict of interest.

Author contributions

Conceptualization: Simone Micalizzi, Lara Russo, Martina Nencioni

Data curation: Simone Micalizzi, Lara Russo, Martina Nencioni

Formal analysis: Simone Micalizzi, Lara Russo, Martina Nencioni

Funding acquisition: Maria Letizia Trincavelli, Giovanni Vozzi

Investigation: Simone Micalizzi, Lara Russo, Martina Nencioni

Methodology: Simone Micalizzi, Lara Russo, Chiara Giacomelli, Francesca Montemurro, Carmelo de Maria, Martina Nencioni, Laura Marchetti, Maria Letizia Trincavelli, Giovanni Vozzi

Project administration: Maria Letizia Trincavelli, Giovanni Vozzi

Resources: Maria Letizia Trincavelli, Giovanni Vozzi

Supervision: Chiara Giacomelli, Laura Marchetti, Francesca Montemurro, Carmelo de Maria, Maria Letizia Trincavelli, Giovanni Vozzi

Validation: Chiara Giacomelli, Laura Marchetti, Francesca Montemurro, Carmelo de Maria

Visualization: Simone Micalizzi, Lara Russo, Martina Nencioni

Writing – original draft: Simone Micalizzi, Lara Russo, Martina Nencioni

Writing – review & editing: Chiara Giacomelli, Laura Marchetti, Francesca Montemurro, Carmelo de Maria, Maria Letizia Trincavelli, Giovanni Vozzi

Ethics approval and consent to participate

Not applicable.

Consent for publication

Not applicable.

Availability of data

The data presented in this study are available from the corresponding author upon reasonable request.

References

1. Benjamin M, Kumai T, Milz S, *et al.*, 2002, The skeletal attachment of tendons - Tendon 'entheses'. *Comp Biochem Physiol*, 133(4): 931–945.

   https://doi.org/10.1016/S1095-6433(02)00138-1

2. Paxton JZ, Baar K, Grover LM, 2013, Current progress in enthesis repair: Strategies for interfacial tissue engineering. *Orthop Muscular Syst*, 01(S1): 1–13.

   https://doi.org/10.4172/2161-0533.s1-003

3. Golman M, Birman V, Thomopoulos S, 2021, Enthesis strength, toughness and stiffness: An image-based model comparing tendon insertions with varying bony attachment geometries. *J R Soc Interface*, 18(185).

   https://doi.org/10.1098/rsif.2021.0421

4. Benjamin M, Ralphs JR, 1998, Fibrocartilage in tendons and ligaments - An adaptation to compressive load. *J Anat*, 193(4): 481–494.

   https://doi.org/10.1017/S0021878298004300

5. Buenzli PR, Sims NA, 2015, Quantifying the osteocyte network in the human skeleton. *Bone*, 75: 144–150.

   https://doi.org/10.1016/j.bone.2015.02.016

6. Schwartz AG, Long F, Thomopoulos S, 2015, Enthesis fibrocartilage cells originate from a population of hedgehog-responsive cells modulated by the loading environment. *Development*, 142(1): 196–206.

   https://doi.org/10.1242/dev.112714

7. Benjamin M, McGonagle D, 2009, The enthesis organ concept and its relevance to the spondyloarthropathies. *Adv Exp Med Biol*, 649: 57–70.

   https://doi.org/10.1007/978-1-4419-0298-6_4

8. Foolen J, Wunderli SL, Loerakker S, *et al.*, 2018, Tissue alignment enhances remodeling potential of tendon-derived cells - Lessons from a novel microtissue model of tendon scarring. *Matrix Biol*, 65: 14–29.

   https://doi.org/10.1016/j.matbio.2017.06.002

9. Nowlin J, Bismi MA, Delpech B, *et al.*, 2018, Engineering the hard–soft tissue interface with random-to-aligned nanofiber scaffolds. *Nanobiomedicine*, 5: 184954351880353.

   https://doi.org/10.1177/1849543518803538

10. Xie J, Ma B, Michael PL, *et al.*, 2012, Fabrication of nanofiber scaffolds with gradations in fiber organization and their potential applications. *Macromol Biosci*, 12(10): 1336–1341.

    https://doi.org/10.1002/mabi.201200115

11. Xiong J, Wang H, Lan X, *et al.*, 2022, Fabrication of bioinspired grid-crimp micropatterns by melt electrospinning writing for bone-ligament interface study. *Biofabrication*, 14(2): 025008–025008.

    https://doi.org/10.1088/1758-5090/ac4ac8

12. Criscenti G, Longoni A, Di Luca A, *et al.*, 2016, Triphasic scaffolds for the regeneration of the bone-ligament interface. *Biofabrication*, 8(1): 15009.

    https://doi.org/10.1088/1758-5090/8/1/015009

13. Silva M, Ferreira FN, Alves NM, *et al.*, 2020, Biodegradable polymer nanocomposites for ligament/tendon tissue engineering. *J Nanobiotechnol*, 18(1): 1–33.

https://doi.org/10.1186/s12951-019-0556-1

14. Barber JG, Handorf AM, Allee TJ, *et al.*, 2013, Braided nanofibrous scaffold for tendon and ligament tissue engineering. *Tissue Eng Part A*, 19(11–12): 1265–1274.

https://doi.org/10.1089/ten.tea.2010.0538

15. Sahoo S, Ouyang H, James CH, *et al.*, 2006, Characterization of a novel polymeric scaffold for potential application in tendon/ligament tissue engineering. *Tissue Eng*, 12(1): 91–99.

https://doi.org/10.1089/ten.2006.12.91

16. Jayasree A, Thankappan SK, Ramachandran R, *et al.*, 2019, Bioengineered braided micro-nano (multiscale) fibrous scaffolds for tendon reconstruction. *ACS Biomater Sci Eng*, 5(3): 1476–1486.

https://doi.org/10.1021/acsbiomaterials.8b01328

17. Tsutsumi H, Kurimoto R, Nakamichi R, *et al.*, 2022, Generation of a tendon-like tissue from human iPS cells. *J Tissue Eng*, 13: 1–5.

https://doi.org/10.1177/20417314221074018

18. Costa-Almeida R, Calejo I, Gomes ME, 2019, Mesenchymal stem cells empowering tendon regenerative therapies. *Int J Mol Sci*, 20(12): 3002–3002.

https://doi.org/10.3390/ijms20123002

19. Trincavelli ML, Daniele S, Giacomelli C, *et al.*, 2014, Osteoblast differentiation and survival: A role for A2B adenosine receptor allosteric modulators. *Biochim Biophys Acta Mol Cell Res*, 1843(12): 2957–2966.

https://doi.org/10.1016/j.bbamcr.2014.09.013

20. Luo W, Wang Y, Han Q, *et al.*, 2022, Advanced strategies for constructing interfacial tissues of bone and tendon/ligament. *J Tissue Eng*, 13: 1–31.

https://doi.org/10.1177/20417314221144714

21. Yang G, Lin H, Rothrauff BB, *et al.*, 2016, Multilayered polycaprolactone/gelatin fiber-hydrogel composite for tendon tissue engineering. *Acta Biomater*, 35: 68–76.

https://doi.org/10.1016/j.actbio.2016.03.004

22. Cao Y, Yang G, Lin H, *et al.*, 2020, Three-dimensional printed multiphasic scaffolds with stratified cell-laden gelatin methacrylate hydrogels for biomimetic tendon-to-bone interface engineering. *J Orthop Transl*, 23(January): 89–100.

https://doi.org/10.1016/j.jot.2020.01.004

23. Yin Z, Chen X, Chen JL, *et al.*, 2010, The regulation of tendon stem cell differentiation by the alignment of nanofibers. *Biomaterials*, 31(8): 2163–2175.

https://doi.org/10.1016/j.biomaterials.2009.11.083

24. Chen YC, Lin R-Z, Qi H, *et al.*, 2012, Functional human vascular network generated in photocrosslinkable gelatin methacrylate hydrogels. *Adv Funct Mater*, 22(10): 2027–2039.

https://doi.org/10.1002/adfm.201101662

25. Pulidori E, Micalizzi S, Bramanti E, *et al.*, 2021, One-pot process: Microwave-assisted keratin extraction and direct electrospinning to obtain keratin-based bioplastic. *Int J Mol Sci*, 22(17): 9597.

https://doi.org/10.3390/ijms22179597

26. Nichol JW, Koshy ST, Bae H, *et al.*, 2010, Cell-laden microengineered gelatin methacrylate hydrogels. *Biomaterials*, 31(21): 5536–5544.

https://doi.org/10.1016/j.biomaterials.2010.03.064

27. Maniruzzaman M, Boateng JS, Snowden MJ, *et al.*, 2012, A review of hot-melt extrusion: process technology to pharmaceutical products. *ISRN Pharm*, 2012: 1–9.

https://doi.org/10.5402/2012/436763

28. Temple JP, Hutton DL, Hung BP, *et al.*, 2014, Engineering anatomically shaped vascularized bone grafts with hASCs and 3D-printed PCL scaffolds. *J Biomed Mater Res Part A*, 102(12): 4317–4325.

https://doi.org/10.1002/jbm.a.35107

29. Amiel D, Frank C, Harwood F, *et al.*, 1984, Tendons and ligaments: A morphological and biochemical comparison. *J Orthop Res*, 1: 251–265.

30. You Y, Lee SJ, Min BM, *et al.*, 2006, Effect of solution properties on nanofibrous structure of electrospun poly(lactic-co-glycolic acid). *J Appl Polym Sci*, 99(3): 1214–1221.

https://doi.org/10.1002/app.22602

31. Sato K, Yu Q, Hiramoto J, *et al.*, 2015, A method to investigate strain rate effects on necking and fracture behaviors of advanced high-strength steels using digital imaging strain analysis. *Int J Impact Eng*, 75: 11–26.

https://doi.org/10.1016/j.ijimpeng.2014.07.001

32. Peters WH, Ranson WF, 1982, Digital imaging techniques in experimental stress analysis. *Opt Eng*, 21(3): 213427.

33. Barresi E, Giacomelli C, Marchetti L, *et al.*, 2021, Novel positive allosteric modulators of A2B adenosine receptor acting as bone mineralisation promoters. *J Enzyme Inhib Med Chem*, 36(1): 286–294. 10.1080/14756366.2020.1862103

34. Sry V, Mizutani Y, Endo G, *et al.*, 2018, Estimation of the longitudinal elasticity modulus of braided synthetic fiber rope utilizing classical laminate theory with the unit N/tex. *Appl Sci*, 8(7): 1096–1096.

https://doi.org/10.3390/app8071096

35. Kempfert M, Willbold E, Loewner S, *et al.*, 2022, Polycaprolactone-based 3D-printed scaffolds as potential implant materials for tendon-defect repair. *J Funct Biomater*, 13(4): 160.

https://doi.org/10.3390/jfb13040160

36. Guedes F, Branquinho MV, Biscaia S, *et al.*, 2022, Gamma irradiation processing on 3D PCL devices: A preliminary biocompatibility assessment. *Int J Mol Sci*, 23(24): 15916–15916.

https://doi.org/10.3390/ijms232415916

37. Giacomelli C, Natali L, Nisi M, *et al.*, 2018, Negative effects of a high tumour necrosis factor-α concentration on human gingival mesenchymal stem cell trophism: The use of natural compounds as modulatory agents. *Stem Cell Res Ther*, 9(1): 1–21.

https://doi.org/10.1186/s13287-018-0880-7

38. Bowers K, Amelse L, Bow A, *et al.*, 2022, Mesenchymal stem cell use in acute tendon injury: In vitro tenogenic potential vs. in vivo dose response. *Bioengineering*, 9(8): 407–407.

https://doi.org/10.3390/bioengineering9080407

39. Zhao Y, Sun Q, Wang S, *et al.*, 2019, Spreading shape and area regulate the osteogenesis of mesenchymal stem cells. *Tissue Eng Regen Med*, 16(6): 573–583.

https://doi.org/10.1007/s13770-019-00213-y

40. Khan AU, Qu R, Fan T, *et al.*, 2020, A glance on the role of actin in osteogenic and adipogenic differentiation of mesenchymal stem cells. *Stem Cell Res Ther*, 11(1): 1–14.

https://doi.org/10.1186/s13287-020-01789-2

41. Siadat SM, Silverman AA, DiMarzio CA, *et al.*, 2021, Measuring collagen fibril diameter with differential interference contrast microscopy. *J Struct Biol*, 213(1): 1–17.

https://doi.org/10.1016/j.jsb.2021.107697

42. Nazeri N, Derakhshan MA, Faridi-Majidi R, *et al.*, 2018, Novel electro-conductive nanocomposites based on electrospun PLGA/CNT for biomedical applications. *J Mater Sci Mater Med*, 29(11): 1–9.

https://doi.org/10.1007/s10856-018-6176-8

43. Chou SF,. Woodrow KA, 2017, Relationships between mechanical properties and drug release from electrospun fibers of PCL and PLGA blends. *J Mech Behav Biomed Mater*, 65(September 2016): 724–733.

https://doi.org/10.1016/j.jmbbm.2016.09.004

44. Górecka Ż, Idaszek J, Kołbuk D, *et al.*, 2020, The effect of diameter of fibre on formation of hydrogen bonds and mechanical properties of 3D-printed PCL. *Mater Sci Eng C*, 114(April): 111072.

https://doi.org/10.1016/j.msec.2020.111072

45. Brennan DA, Conte AA, Kanski G, *et al.*, 2018, Mechanical considerations for electrospun nanofibers in tendon and ligament repair. *Adv Healthc Mater*, 7(12): 1–31.

https://doi.org/10.1002/adhm.201701277

46. Shin HJ, Lee CH, Cho IH, *et al.*, 2006, Electrospun PLGA nanofiber scaffolds for articular cartilage reconstruction: Mechanical stability, degradation and cellular responses under mechanical stimulation in vitro. *J Biomater Sci Polym Ed*, 17(1): 103–119.

https://doi.org/10.1163/156856206774879126

47. Sperling LE, Reis KP, Pozzobon LG, *et al.*, 2017, Influence of random and oriented electrospun fibrous poly(lactic-co-glycolic acid) scaffolds on neural differentiation of mouse embryonic stem cells. *J Biomed Mater Res Part A*, 105(5): 1333–1345.

https://doi.org/10.1002/jbm.a.36012

48. Balestri W, Hickman GJ, Morris RH, *et al.*, 2023, Triphasic 3D in vitro model of bone-tendon-muscle interfaces to study their regeneration. *Cells*, 12(2): 313–313.

https://doi.org/10.3390/cells12020313

49. Fazeli N, Arefian E, Irani S, *et al.*, 2021, 3D-printed PCL scaffolds coated with nanobioceramics enhance osteogenic differentiation of stem cells. *ACS Omega*, 6(51): 35284–35296.

https://doi.org/10.1021/acsomega.1c04015

50. Ramakrishna H, Li T, He T, *et al.*, 2019, Tissue engineering a tendon-bone junction with biodegradable braided scaffolds. *Biomater Res*, 23(1): 1–12.

https://doi.org/10.1186/s40824-019-0160-3

51. Rinoldi C, Fallahi A, Yazdi IK, *et al.*, 2019, Mechanical and biochemical stimulation of 3D multilayered scaffolds for tendon tissue engineering. *ACS Biomater Sci Eng*, 5(6): 2953–2964.

https://doi.org/10.1021/acsbiomaterials.8b01647

52. De Maria C, Giusti S, Mazzei D, *et al.*, 2011, Squeeze pressure bioreactor: A hydrodynamic bioreactor for noncontact stimulation of cartilage constructs. *Tissue Eng Part C Methods*, 17(7): 757–764.

https://doi.org/10.1089/ten.tec.2011.0002

53. Banik BL., Brown JL, 2020, 3D-printed bioreactor enhances potential for tendon tissue engineering. *Regen Eng Transl Med*, 6(4): 419–428.

https://doi.org/10.1007/s40883-019-00145-y